

The metallicity of circumnuclear star forming regions

By Ángeles I. Díaz¹
Elena Terlevich²
Marcelo Castellanos^{1,3}
Guillermo Hägele¹

¹ Universidad Autónoma de Madrid, Spain

² Instituto Nacional de Astrofísica, Óptica y Electrónica, Puebla, México

³ Instituto de Estructura de la Materia, CSIC, Madrid, Spain

We present a spectrophotometric study of circumnuclear star forming regions (CNSFR) in the early type spiral galaxies: NGC 2903, NGC 3351 and NGC 3504, all of them of over solar metallicity according to standard empirical calibrations. A detailed determination of their abundances is made after careful subtraction of the very prominent underlying stellar absorption. It is found that most regions show the highest abundances in HII region-like objects. The relative N/O and S/O abundances are discussed. It is also shown that CNSFR, as a class, segregate from the disk HII region family, clustering around smaller “softness parameter” – η' – values, and therefore higher ionizing temperatures.

1. Introduction

The inner parts of some spiral galaxies show higher star formation rates than usual and this star formation is frequently arranged in a ring or pseudo-ring pattern around their nuclei. In general, Circumnuclear Star Forming Regions (CNSFR), also referred to as “hotspots”, are alike luminous and large disk HII regions, but look more compact and show higher peak surface brightness (Kennicutt et al. 1989). In many cases they contribute substantially to the UV emission of the entire nuclear region (*e.g.* Colina et al. 2002). Their H α luminosities overlap with those of HII galaxies being typically higher than 10^{39} erg s^{−1} which points to relatively massive ionizing star clusters. These regions are expected to show a high metallicity as corresponds to their position near the galactic bulge. They have considerable weight in the determination of abundance gradients, which in turn are widely used to constrain chemical evolution models, and constitute excellent laboratories to study how star formation proceeds in high metallicity environments.

2. Observations and reductions

12 CNSFRs were observed with the 4.2m WHT at the Roque de los Muchachos Observatory using the ISIS double spectrograph, with the EEV12 and TEK4 detectors in the blue and red arm respectively with the dichroic at $\lambda 7500$ Å. Gratings R300B in the blue arm and R600R in the red arm were used, covering the spectral ranges $\lambda 3650 - \lambda 7000$ Å in the blue and ($\lambda 8850 - \lambda 9650$) in the near IR, yielding spectral dispersions of 1.73 Å pixel^{−1} in the blue arm and 0.79 Å pixel^{−1} in the red arm. A slit width of 1 arcsec was used. The nominal spatial sampling was 0.4 arcsec pixel^{−1} in each frame and the average seeing for this night was ~ 1.2 arcsec.

The data were reduced using the IRAF (Image Reduction and Analysis Facility) package following standard procedures. The high spectral dispersion used in the near infrared allowed the almost complete elimination of the night-sky OH emission lines and, in fact,

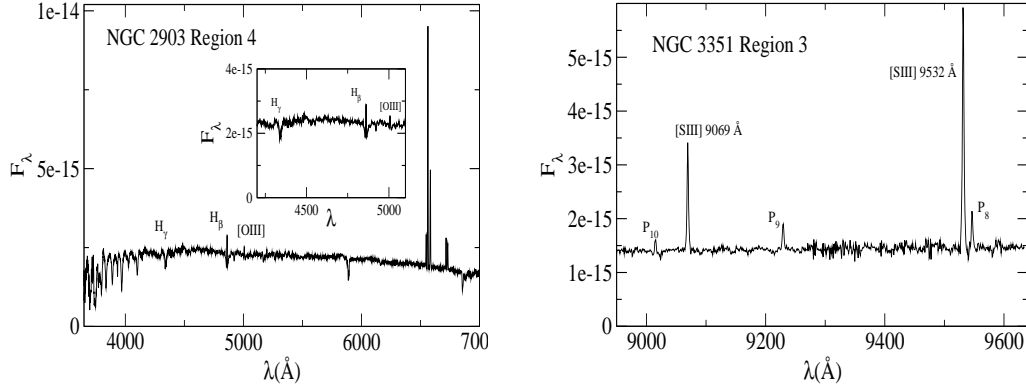


FIGURE 1. *Left panel:* Blue spectrum of region 4 in NGC 2903 *Right panel:* Red spectrum of region 3 in NGC 3351.

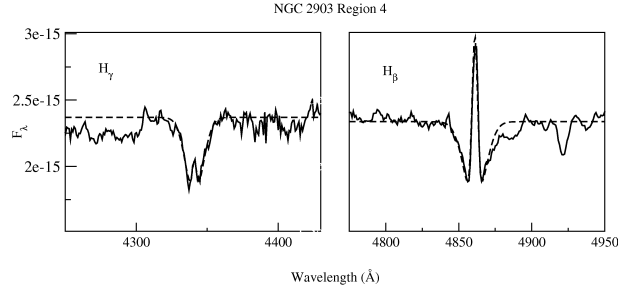


FIGURE 2. Example of the fitting procedure used in order to correct the Balmer emission line intensities for the presence of the underlying stellar population.

the observed $\lambda 9532/\lambda 9069$ ratio is close to the theoretical value of 2.48 in all cases. Telluric absorptions have been removed from the spectra of the regions by dividing by a relatively featureless continuum of a subdwarf star observed in the same night.

3. Results and discussion

Examples of blue and red spectra are shown in Figure 1. Emission line fluxes were measured using the IRAF SPLIT software package. The presence of a conspicuous underlying stellar population, more evident in the blue spectra, in most observed regions complicates the measurements. An example of underlying absorption can be seen in the inset to the left panel of Figure 1. A two-component (emission and absorption) gaussian fit was performed in order to correct the Balmer lines for underlying absorption. An example of this procedure is shown in Figure 2.

The low excitation of the regions, as evidenced by the weakness of the [OIII] $\lambda 5007$ Å line (see left panel of Figure 1), precludes the detection and measurement of the auroral [OIII] $\lambda 3463$ Å necessary for the derivation of the electron temperature. It is therefore impossible to obtain a direct determination of the oxygen abundances. Empirical calibrations have to be used instead. In the left panel of Figure 3 we show the calibration of oxygen abundance by the commonly used O_{23} parameter defined as $([OII]\lambda 3727, 29 + [OIII]\lambda 4959, 5007)/H_{\beta}$ (Pagel et al. 1979). Data on HII galaxies, disc HII regions and CNSFR are shown. The HII region sample (Pérez-Montero & Díaz 2005) has been divided in under-solar (open triangles) and over-solar (filled triangles) according

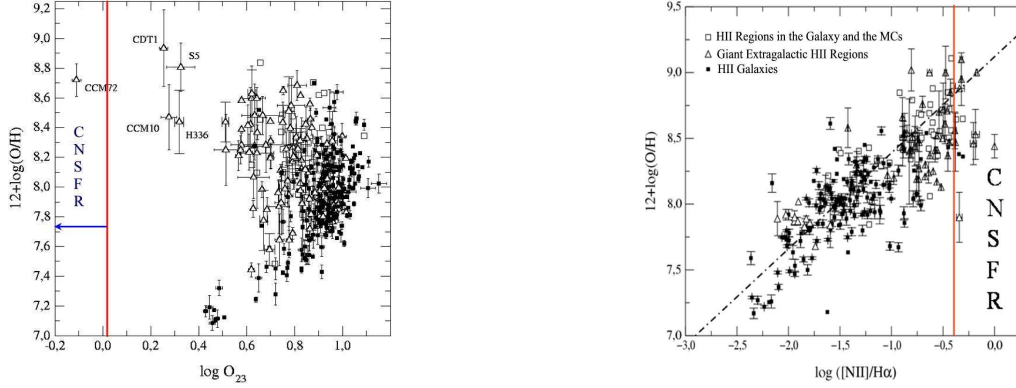


FIGURE 3. *Left panel:* The O_{23} abundance parameter calibration. *Right panel:* The $N2$ abundance parameter calibration. The location of CNSFR is indicated

to the empirical criterion given by Díaz & Pérez-Montero (2000), *i. e.* $O_{23} \leq 0.47$ and $-0.5 \leq S_{23} \leq 0.28$ †. The HII galaxy data (filled squares) come from Pérez-Montero & Díaz (2003). CNSFR are represented by circles. Solid ones for our observed objects and open ones for regions in NGC 3310 and NGC 7714, known to have under-solar abundances (Pastoriza et. 1993; González-Delgado et al. 1995). As can be seen the calibration is two-folded, shows a considerable scatter and its high abundance end is not well sampled. The position of the observed CNSFR is indicated. Their observed O_{23} values, lower than those of the lowest abundance galaxy known (IZw18), indicates that CNSFR belong to the high abundance branch of the calibration showing possibly the highest metallicities shown by HII region like objects. In the right panel of Figure 3 the position of the regions is indicated in the $N2$ ($[\text{NII}]/\text{H}\alpha$) abundance calibration diagram (Denicoló et al. 2002), which shows a linear behaviour. Again CNSFR appear to show the highest oxygen abundances.

The left panel of Figure 4 shows the $[\text{NII}]/[\text{OII}]$ ratio *versus* the $N2$ abundance parameter. Since a good correlation has been found to exist between the $[\text{NII}]/[\text{OII}]$ ratio and the N^+/O^+ ionic abundance ratio, which in turn can be assumed to measure the N/O ratio, this graph is the observational equivalent of the N/O *vs* O/H diagram. We can see that a very tight correlation exists for all represented objects: HII galaxies, low and high abundance HII regions and CNSFR. Again our observed regions show the highest N/O ratios of the sample.

The right panel of Figure 4 shows the run of the excitation degree with metallicity for the observed regions through the $[\text{SII}]/[\text{SIII}]$ ratio, which has been shown to be a good ionization parameter indicator (Díaz et al. 1991), and the $N2$ parameter. It can be seen that the observed CNSFR show the lowest excitation of the sample.

A hint on the ionizing temperature of the regions can be obtained through the use of the η' parameter, which is a measure of the softness of the ionizing radiation (see Vílchez & Pagel 1988) and increases with decreasing ionizing temperature. The left panel of Figure 5 shows the run of η' with metallicity as parametrized by $N2$. Unexpectedly, CNSFR show values of η' higher than those of over-solar disc HII regions. This is better appreciated in the right panel of the figure where CNSFR are seen to segregate from disc HII regions in the $[\text{OII}]/[\text{OIII}]$ *vs* $[\text{SII}]/[\text{SIII}]$ diagram. The former cluster around the value of $\log \eta' = 0.0$ ($T_{\text{ion}} \sim 40,000$ K) while the latter cluster around $\log \eta' = 0.8$ ($T_{\text{ion}} \sim 35,000$ K).

† The sulphur abundance parameters S_{23} is defined as $([\text{SII}] + [\text{SIII}])/H_{\beta}$

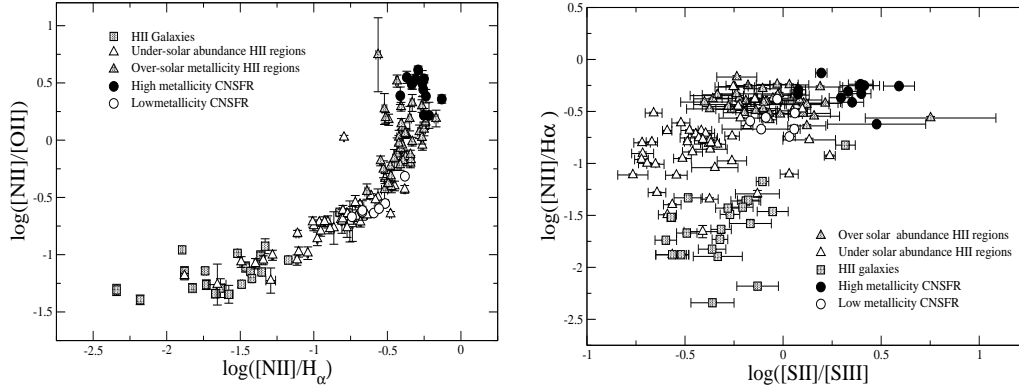


FIGURE 4. *Left panel:* Empirical version of the N/O vs O/H relation. *Right panel:* The N2 abundance parameter as a function of excitation, as measured by the [SII]/[SIII] ratio.

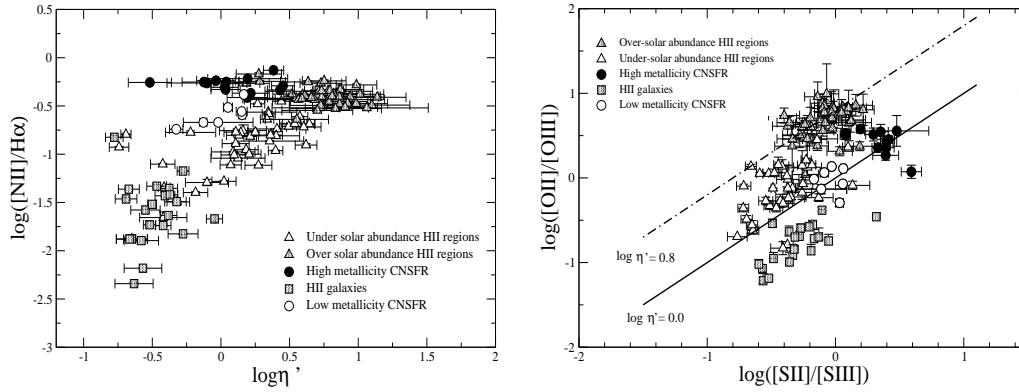


FIGURE 5. *Left panel:* The N2 vs η' relation. *Right panel:* Logarithmic relation between the [OII]/[OIII] and [SII]/[SIII] line ratios

This work has been supported by Spanish projects DGICYT- AYA-2004-08262-C03-03 and CM-ASTROCAM.

REFERENCES

- Colina, L., González-Delgado, R., Mas-Hesse, J. M. & Leitherer, C. (2002). *ApJ* **579**, 545-553.
 Denicoló, G., Terlevich, R. & Terlevich, E. (2002) *MNRAS* **330**, 69-74.
 Díaz, A.I. & Pérez-Montero, E. (2000) *MNRAS* **135**, 130-138.
 González-Delgado, R., Pérez, E., Díaz, A.I., García-Vargas, M.L., Terlevich, E. & Vílchez, J.M. (1995). *ApJ* **439**, 604-622.
 Kennicutt, R.C., Keel, W.C. & Blaha, C.A. (1989). *AJ* **97**, 1022-1035.
 Pagel, B.E.J., Edmunds, M.G., Edmunds, M. G., Blackwell, D. E., Chun, M. S.; Smith, G. (1979). *MNRAS* **185**, 95-113.
 Pastoriza, M. G., Dottori, H. A., Terlevich, E., Terlevich, R., Diaz, I. (1993) *MNRAS* **260**, 177-190.
 Pérez-Montero & Díaz, A.I. (2003) *MNRAS* **346**, 105-118.
 Pérez-Montero & Díaz, A.I. (2005) *MNRAS* **361**, 1063-1076.
 Vílchez, J.M. & Pagel, B.E.J. (1988) *MNRAS*, **231**, 257-267.